Computers and Mathematics with Applications 61 (2011) 2843–2853

Contents lists available at ScienceDirect

Computers and Mathematics with Applications

journal homepage: www.elsevier.com/locate/camwa

An image reconstruction algorithm based on the semiparametric model for electrical capacitance tomography

J. Lei [a,*], S. Liu [a], H.H. Guo [b], Z.H. Li [a], J.T. Li [a], Z.X. Han [a]

[a] *Key Laboratory of Condition Monitoring and Control for Power Plant Equipment, Ministry of Education, North China Electric Power University, Changping District, Beijing 102206, China*

[b] *College of Economics, Jinan University, Guangzhou 510632, China*

ARTICLE INFO

Article history:
Received 10 August 2009
Received in revised form 17 March 2011
Accepted 17 March 2011

Keywords:
Electrical capacitance tomography
Image reconstruction
Semiparametric model
Homotopy method

ABSTRACT

Electrical capacitance tomography (ECT) is considered as a promising tomography technology, and exactly reconstructing the original objects is highly desirable in real applications. In this paper, a generalized image reconstruction model that simultaneously considers the inaccurate property in the measured capacitance data and the linearization approximation error is presented. A generalized objective function, which has been developed using a combinational M-estimation and an extended stabilizing item, is proposed. The objective function unifies six estimation methods into a concise formula, where different estimation methods can be easily obtained by selecting different parameters. The homotopy method that integrates the beneficial advantages of the alternant iteration scheme is employed to solve the proposed objective function. Numerical simulations are implemented to evaluate the numerical performances and effectiveness of the proposed algorithm, and the numerical results reveal that the proposed algorithm is efficient and overcomes the numerical instability in the process of ECT image reconstruction. For the reconstructed objects in this paper, a dramatic improvement in accuracy and spatial resolution can be achieved, which indicates that the proposed algorithm is a promising candidate for solving ECT inverse problems.

1. Introduction

Applying the process tomography (PT) techniques to investigate the dynamic behaviors of multiphase systems in industrial processes to reduce pollutant emission, improve efficiency and save energy has attracted widespread attention in the past few years. Successful applications of the PT techniques depend mainly on the selection of the sensor system deployed for the specified applications and the image reconstruction algorithms. ECT technology attempts to reconstruct the cross-sectional permittivity distribution of a dielectric object from a set of the measured capacitance data. Owing to the distinct advantages such as non-intrusive sensing, high speed, low cost, easy implementation and high safety, ECT is regarded as a promising PT technology. In recent years, ECT technology has been accepted as a potent laboratory tool for the investigation of the dynamic behaviors of multiphase systems or processes, and the identification of two-phase flow patterns [1–10]. Furthermore, the application areas are being exploited.

Image reconstruction algorithms play a vital role in the successful application of ECT technology. Unfortunately, solutions to the ECT inverse problem have to cope with a fundamental difficulty derived from the ill-posed nature, i.e., small perturbations in the measured data or the forward solution will bring about unacceptably large errors in the inverse

* Corresponding author. Tel.: +86 10 61772472; fax: +86 10 61772219.
E-mail address: leijing2002@126.com (J. Lei).

0898-1221/$ – see front matter © 2011 Elsevier Ltd. All rights reserved.
doi:10.1016/j.camwa.2011.03.060

solutions. At present, the most crucial problems that still challenge the applications of ECT may be the relatively low spatial resolution and accuracy in the reconstructed images. In ECT applications, it is exceedingly desirable to reconstruct images with high accuracy. As a result, finding ways to improve ECT reconstruction quality has attracted widespread attention in the past few years, and various algorithms had been proposed for ECT image reconstruction, such as the linear back-projection (LBP) method [11], the Tikhonov regularization method [12], the Landweber iteration algorithm [13–17], the truncated singular value decomposition (TSVD) method [13,17], the algebraic reconstruction technique (ART) method [17], the simultaneous iterative reconstruction technique (SIRT) [18], the genetic algorithm [19], the generalized vector sampled pattern matching method [20], the generalized Tikhonov regularization method [21–23], the simulated annealing algorithm [24], the neural network algorithm [25,26], the OIOR algorithm [27], the Helmholtz-type regularization method [28] and the four-dimensional reconstruction method [29]. It is worth mentioning that the Tikhonov regularization method, the Landweber iteration algorithm and the TSVD method are three kinds of typical regularization techniques. The distinct advantages of the LBP method are the numerical simplicity, and computational efficiency resulting from it only involving a single matrix–vector multiplication; in particular the method can achieve online reconstruction. Unfortunately, the quality of the images reconstructed by the LBP method is relatively low for complicated reconstruction tasks. As a result, the LBP method is often applied in the qualitative analysis. The Landweber iteration algorithm has seen widespread application in the past few years. The remarkable benefits of this algorithm include the easy implementation and low computational complexity and cost. In most cases, the method is often effective. From the viewpoint of numerical optimization, however, it is only a steepest descent algorithm, the rate of convergence is relatively low and the search process often falls into the attractive domain of a local optimal solution. As a result, the accuracy of the images reconstructed by the Landweber iteration algorithm is limited. The standard Tikhonov regularization (STR) method is an efficient approach for solving inverse problems and has been successfully applied in various fields, with favorable numerical performances. In essence, a Tikhonov regularization solution is a result of balancing the accuracy and stability of a solution. When the STR method is applied in ECT image reconstruction, however, the quality of the images reconstructed by the algorithm is far from perfect owing to the excessive smoothness effect. A distinct property of the STR method is achieving online reconstruction, which is very important for some special applications. Additionally, it is worth mentioning that selecting a suitable regularization parameter is a challenging task for successful application of the STR method. The TSVD method achieves numerical stability of a solution by truncating the small singular values of the coefficient matrix [17]. The advantages for the method involve the easy implementation and low computational complexity; unfortunately, determining the truncated singular values is challenging, particularly when the singular values of the coefficient matrix are continuously descendent. In addition, when a large scale problem is considered, the computational burden in implementing the SVD is heavy. As a result, the TSVD method is seldom adopted in the field of ECT image reconstruction. The ART algorithm and the SIRT algorithm are commonly used for image reconstruction in X-ray computerized tomography. They are simple and effective, especially when the system matrix is very large. Unfortunately, the quality of the images reconstructed by the ART algorithm and the SIRT algorithm are not satisfactory in ECT applications. The four-dimensional reconstruction method can achieve four-dimensional dielectric permittivity imaging using multi-frame ECT data, which provides a promising approach for improving the spatial resolution of the reconstructed images [29].

In the past few years, these algorithms have played a positive role in promoting the development of ECT technology and expanding the ranges of application. However, applications reveal that each algorithm has its pros and cons, and may show different numerical performances for different reconstruction tasks. As a result, in real applications the selection of a suitable algorithm depends greatly on the measurement requirements and the prior information for a specific reconstruction objective. By and large, ECT reconstruction algorithms are far from perfect, and finding an efficient algorithm for achieving a dramatic improvement in the reconstruction quality is highly desirable.

On the basis of the semiparametric method, this paper presents a generalized reconstruction model that simultaneously considers the errors in the measured capacitance data and the linearization approximation error. A generalized objective function, which has been developed using a combinational M-estimation and an extended stabilizing item, is proposed. The objective function unifies six estimation methods into a concise formula, where different estimation methods can be easily obtained by choosing different parameters. The homotopy method that integrates the desirable advantages of the alternant iteration scheme is introduced for solving the proposed objective function. Numerical simulations were implemented to evaluate the numerical performances and the effectiveness of the proposed algorithm, and satisfactory numerical performances and encouraging results are observed.

The rest of this paper is organized as follows. Section 2 introduces the semiparametric model and a concise comparison between the linearization model and the semiparametric model is presented. In Section 3, a generalized objective function, which has been developed using combinational M-estimation and an extended stabilizing item, is described in detail. In Section 4, the homotopy method that integrates the beneficial advantage of the alternant iteration scheme is introduced, for solving the proposed objective function problem. The numerical simulation results are presented in Section 5, for illustration. Finally, Section 6 provides a summary and conclusion.

2. Representation of the ECT model

Roughly speaking, two problems, the forward problem and the inverse problem, arise in the process of ECT image reconstruction. The main task of ECT forward problem solving is to compute the inter-electrode capacitances from the

known permittivity distribution; in this phase the numerical implementation is relatively easy. The inverse problem aims to estimate the permittivity distribution from the known capacitance data. In real applications, taking the measurement noises and the linearization approximation into account, the ECT image reconstruction model can be simplified to [17]

$$SG = C + d \tag{1}$$

where: C is an $m \times 1$-dimensional vector indicating the normalized capacitance values; G is an $n \times 1$-dimensional vector standing for the normalized permittivity distribution, which denotes the gray level values in the reconstructed image; S represents a matrix of dimension $m \times n$; d stands for an $m \times 1$-dimensional vector indicating the noises in the capacitance data.

It can be found from Eq. (1) that in the traditional linear model the higher order items are omitted in the process of linearization. Applications indicate that the linearization model is feasible when the contrast between the low permittivity and high permittivity in the reconstructed region is small, and has seen many successful applications. However, the linearization model may yield a large approximation error when the difference between the low permittivity and high permittivity in the reconstructed region is large. At present, the nonlinear reconstruction algorithms have been developed for ECT image reconstruction [21,23]. Unfortunately, the computational burden and complexity is relatively high. Therefore, developing an efficient algorithm with low computational cost and complexity for simultaneously treating the inaccuracies in the capacitance data and the image reconstruction model is highly desirable for real applications. The semiparametric model simultaneously considers the noises in the measured capacitance data and the linearization approximation errors, which can be formulated as [30]

$$SG + B = C + r \tag{2}$$

where B is an $m \times 1$-dimensional vector indicating the linearization error and r stands for an $m \times 1$-dimensional vector indicating the noises in the capacitance data. In this work, Eq. (2) is employed to serve as the image reconstruction model.

Comparing Eqs. (1) and (2), it can be seen that Eq. (2) is equivalent to Eq. (1) when $B = 0$. It is obvious that Eq. (1) is a special case of Eq. (2). In Eq. (2), the major task of ECT inverse problem solving is obtaining G and B from the known S and C parameters. It is worth noting that as compared to those for direct nonlinear image reconstruction algorithms, the computational cost and complexity of the semiparametric model are relatively low, when simultaneously considering the noise in the capacitance data and the linearization approximation error; furthermore, the numerical implementation is comparatively easy, which will facilitate real engineering applications.

3. Algorithm analysis

Eq. (2) introduces an alternative model for ECT image reconstruction. It is obvious that finding an efficient computational method is essential for the successful application of Eq. (2). It is well known that the process of ECT image reconstruction is a typical ill-posed problem. In order to obtain a physically meaningful solution, as a consequence, methods that ensure a stable numerical solution while increasing the quality of the reconstructed images should be employed. Applications indicate that the ECT image reconstruction process is often reformulated into an optimization problem. As a result, a key issue, that of how to design an efficient objective function, arises. In this section, a generalized objective function which has been developed using a combinational M-estimation and an extended stabilizing item is described in detail.

3.1. The regularized semiparametric method

Directly solving Eq. (2) is challenging because two unknown variables G and B need to be obtained. An efficient approach is to reformulate the solving of Eq. (2) into an optimization problem. In [31], the authors proposed the regularized semiparametric method, which can be described as follows:

$$\min_{G,B} J = \|E\,(SG + B - C)\|^2 + \alpha_1 \|QB\|^2 + \alpha_2 \|RG\|^2 \tag{3}$$

where: α_1 and α_2 are the regularization parameters; $\|\cdot\|$ defines the 2-norm; and E, Q and R are weighted matrices. It can be seen that Eq. (3) is a special case of the Tikhonov regularization method, and the approximate solution obtained is a result of balancing the accuracy and stability of a solution.

3.2. Extension of the objective function

Design of a favorable Tikhonov regularization objective function includes two key issues: the choice of the measure function of accuracy of a solution and the design of the stabilizing item [12,32,33]. In general, a Tikhonov regularization solution is a result of balancing the accuracy and stability of a solution. According to the basic elements of the Tikhonov regularization method [32], as a consequence, Eq. (3) can be reformulated into a generalized form:

$$\min_{G,B} J = \varphi\,(G, B) + \alpha_1 \Omega_1\,(B) + \alpha_2 \Omega_2\,(G) \tag{4}$$

where $\varphi\,(G, B)$ measures the accuracy of a solution; $\Omega_1\,(B)$ and $\Omega_2\,(G)$ can be referred to as the stabilizing functions.

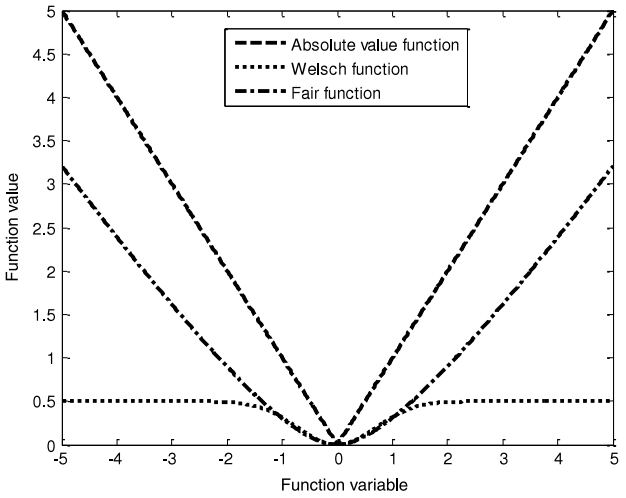

Fig. 1. Function graphs for the absolute value function, the Welsch function and the Fair function.

It can be seen from the first item of the right hand side of Eq. (3) that a function of the sum of squares is used to measure the fidelity of the capacitance data. Unfortunately, the least squares (LS) estimation is sensitive to outliers in the data. In particular, the LS estimation is strongly influenced by the small cluster of outliers [34]. As a consequence, this approach is therefore not directly suitable for the problems of estimations with outliers. Applications indicate that a robustness estimation method, which can achieve a dramatic improvement in the reconstruction quality, will be highly desirable for successful applications of ECT. Consequently, seeking a robust method is crucial for improving the robustness of the LS estimation. In [30], on the basis of the M-estimation, a robust semiparametric estimation had been proposed, which can be expressed as follows:

$$\min_{G,B} J = \sum_{j=1}^{m} \rho\left(S_j G + B_j - C_j\right) \tag{5}$$

where: $\rho(\cdot)$ stands for an M-estimation function; S_j is the jth row of matrix S; and B_j and C_j represent the jth elements of vectors B and C, respectively. Popular M-estimation functions include the absolute value function, the Huber function, the Talvar function, the Welsch function and the Fair function. Fig. 1 presents the function graphs for the absolute value function, the Welsch function and the Fair function when the value of the scale parameter is 1, and more details on the M-estimation functions can be found in [34,35].

In real applications, the distribution patterns and level of the noises in the measured capacitance data are highly complicated. Consequently, deciding how to select a suitable M-estimation function is challenging in real applications. In the field of linear regression, a combinational estimation that integrates the beneficial advantages of the least absolute deviations estimation and the M-estimation had been proposed for improving the robustness of the LS method [36]. In order to improve the adaptability of the estimation, on the basis of the semiparametric model, a combinational estimation that integrates the beneficial advantages of the different M-estimation functions is proposed, which can be expressed as follows:

$$\min_{G,B} J = (1-\delta)\sum_{j=1}^{m} \rho_1\left(S_j G + B_j - C_j\right) + \delta \sum_{j=1}^{m} \rho_2\left(S_j G + B_j - C_j\right) \tag{6}$$

where $0 \leq \delta \leq 1$; $\rho_1(\cdot)$ and $\rho_2(\cdot)$ represent M-estimation functions. It is clear that Eq. (6) integrates the beneficial advantages of two M-estimation functions, which may improve the robustness and adaptability of estimation in real applications. Additionally, it can be seen that in Eq. (6) different estimation methods can be conveniently obtained by selecting different parameters, which is a desirable property for real ECT applications. Taking the ill-posed nature into account, as a result, applying the Tikhonov regularization technique to Eq. (6) yields

$$\min_{G,B} J = (1-\delta)\sum_{j=1}^{m} \rho_1\left(S_j G + B_j - C_j\right) + \delta \sum_{j=1}^{m} \rho_2\left(S_j G + B_j - C_j\right) + \alpha_1 \Omega_1(B) + \alpha_2 \Omega_2(G). \tag{7}$$

The following conclusions can be obtained from Eq. (7):

① Eq. (7) is a regularized robust semiparametric method when $\delta = 1$ and $B \neq 0$, which can be described as follows:

$$\min_{G,B} J = \sum_{j=1}^{m} \rho_2\left(S_j G + B_j - C_j\right) + \alpha_1 \Omega_1(B) + \alpha_2 \Omega_2(G). \tag{8}$$

② Eq. (7) is a regularized robust semiparametric method when $\delta = 0$ and $B \neq 0$, which can be expressed as follows:

$$\min_{G,B} J = \sum_{j=1}^{m} \rho_1 \left(S_j G + B_j - C_j\right) + \alpha_1 \Omega_1 (B) + \alpha_2 \Omega_2 (G) . \tag{9}$$

③ Eq. (7) is a regularized combinational robust semiparametric method when $0 < \delta < 1$ and $B \neq 0$, which can be depicted as follows:

$$\min_{G,B} J = (1-\delta) \sum_{j=1}^{m} \rho_1 \left(S_j G + B_j - C_j\right) + \delta \sum_{j=1}^{m} \rho_2 \left(S_j G + B_j - C_j\right) + \alpha_1 \Omega_1 (B) + \alpha_2 \Omega_2 (G) . \tag{10}$$

④ Eq. (7) is a regularized ordinary M-estimation when $\delta = 1$ and $B = 0$, which can be described as follows:

$$\min_{G} J = \sum_{j=1}^{m} \rho_2 \left(S_j G - C_j\right) + \alpha_2 \Omega_2 (G) . \tag{11}$$

⑤ Eq. (7) is a regularized ordinary M-estimation when $\delta = 0$ and $B = 0$, which can be expressed as follows:

$$\min_{G} J = \sum_{j=1}^{m} \rho_1 \left(S_j G - C_j\right) + \alpha_2 \Omega_2 (G) . \tag{12}$$

⑥ Eq. (7) is a regularized ordinary combinational M-estimation when $0 < \delta < 1$ and $B = 0$, which can be depicted as follows:

$$\min_{G} J = (1-\delta) \sum_{j=1}^{m} \rho_1 \left(S_j G - C_j\right) + \delta \sum_{j=1}^{m} \rho_2 \left(S_j G - C_j\right) + \alpha_2 \Omega_2 (G) . \tag{13}$$

Eq. (7) unifies six regularized estimation methods into a concise formula, where different estimation methods can be easily obtained by selecting different parameters. These properties will be highly desirable for real applications.

The design of the stabilizing item that will strongly influence the quality of the reconstructed images plays an important role in successful applications of Eq. (7). As a consequence, devising an efficient stabilizing item is highly desirable for real applications. Practical experience indicates that the design of the stabilizing item depends mainly on the properties and prior information of a specific reconstruction task. In the past years, various stabilizing items have been developed for ECT image reconstruction. A distinct dissimilarity between different stabilizing items is that different penalties are imposed on the unknown variables to accomplish the numerical stability of a solution from the viewpoint of the penalty function. It is clear that different reconstruction results will be obtained when different stabilizing items are employed. In [37], the following stabilizing function had been proposed for ensuring a stable numerical solution:

$$\Omega (G) = \sum_{i=1}^{n} \frac{G_i^2}{u + G_i^2} \tag{14}$$

where $u > 0$ is a predetermined parameter.

When Eq. (14) is applied in ECT image reconstruction, unfortunately, the quality of the reconstructed images is far from satisfactory owing to the characteristics in the process of ECT image reconstruction. Taking complicated reconstruction objects such as multiphase flows in ECT applications into account, Eq. (14) is generalized to increase the adaptability for complicated reconstruction objects, which can be expressed as follows:

$$\Omega_2 (G) = \sum_{i=1}^{n} \frac{ln\left(1 + ln\left(1 + |G_i|^{p_i}\right)\right)}{u + ln\left(1 + ln\left(1 + |G_i|^{p_i}\right)\right)} \tag{15}$$

where $0 < p_i < 2$. It can be seen from Eqs. (14) and (15) that the two equations are essentially consistent, and the prominent dissimilarity is that different penalties are imposed on the unknown variables to achieve the numerical stability of a solution.

Since the absolute value function is not differentiable at the point when its value is zero. The following formula is employed for approximate computation [38]:

$$|x| \approx \left(x^2 + \xi\right)^{1/2} \tag{16}$$

where $\xi > 0$ is a predetermined parameter. As a result, Eq. (15) can be approximated as follows:

$$\Omega_2 (G) \approx \sum_{i=1}^{n} \frac{ln\left(1 + ln\left(1 + \left(G_i^2 + \xi\right)^{p_i/2}\right)\right)}{u + ln\left(1 + ln\left(1 + \left(G_i^2 + \xi\right)^{p_i/2}\right)\right)} . \tag{17}$$

In this work, the selected M-estimation functions are the Welsch function and the Fair function [34,35], which are presented in Eqs. (18) and (19), respectively:

$$f_{\text{Welsch}}(x) = \frac{\beta_1^2}{2}\left(1 - \exp\left(-\left(\frac{x}{\beta_1}\right)^2\right)\right) \tag{18}$$

$$f_{\text{Fair}}(x) = \beta_2^2\left(\frac{|x|}{\beta_2} - ln\left(1 + \frac{|x|}{\beta_2}\right)\right) \tag{19}$$

where $\beta_1 > 0$ and $\beta_2 > 0$ are the predetermined parameters.

Additionally, in this paper item $\Omega(B)$ is defined as the ℓ_q norm, which can be formulated as follows:

$$\Omega_1(B) = \sum_{j=1}^{m} |B_j|^{q_j} \tag{20}$$

where $0 < q \leq 2$. According to Eq. (16), for easy computation, Eq. (20) can be approximated as follows:

$$\Omega_1(B) \approx \sum_{j=1}^{m} \left(B_j^2 + \xi\right)^{q_j/2}. \tag{21}$$

According to the above discussion, as a result, a generalized objective function can be obtained for ECT image reconstruction:

$$\begin{aligned}\min_{G,B} J = {} & \delta \sum_{j=1}^{m} \frac{\beta_1^2}{2}\left(1 - \exp\left(-\left(\frac{S_jG + B_j - C_j}{\beta_1}\right)^2\right)\right) \\ & + (1-\delta)\sum_{j=1}^{m} \beta_2^2\left(\frac{|S_jG + B_j - C_j|}{\beta_2} - ln\left(1 + \frac{|S_jG + B_j - C_j|}{\beta_2}\right)\right) \\ & + \alpha_1 \sum_{j=1}^{m} |B_j|^{q_j} + \alpha_2 \sum_{i=1}^{n} \frac{ln\left(1 + ln\left(1 + \left(G_i^2 + \xi\right)^{p_i/2}\right)\right)}{u + ln\left(1 + ln\left(1 + \left(G_i^2 + \xi\right)^{p_i/2}\right)\right)}.\end{aligned} \tag{22}$$

According to Eq. (16), for easy computation, Eq. (22) can be approximated as follows:

$$\begin{aligned}\min_{G,B} J = {} & \delta \sum_{j=1}^{m} \frac{\beta_1^2}{2}\left(1 - \exp\left(-\left(\frac{r_j}{\beta_1}\right)^2\right)\right) \\ & + (1-\delta)\sum_{j=1}^{m} \beta_2^2\left(\frac{\left(r_j^2 + \xi\right)^{1/2}}{\beta_2} - ln\left(1 + \frac{\left(r_j^2 + \xi\right)^{1/2}}{\beta_2}\right)\right) + \alpha_1 \sum_{j=1}^{m} \left(B_j^2 + \xi\right)^{q_j/2} \\ & + \alpha_2 \sum_{i=1}^{n} \frac{ln\left(1 + ln\left(1 + \left(G_i^2 + \xi\right)^{p_i/2}\right)\right)}{u + ln\left(1 + ln\left(1 + \left(G_i^2 + \xi\right)^{p_i/2}\right)\right)}\end{aligned} \tag{23}$$

where $r_j = S_jG + B_j - C_j$.

Eqs. (23) and (3) are essentially consistent from the viewpoint of the Tikhonov regularization method, that is, the solution obtained is a result of balancing the accuracy and stability of a solution [32]. The remarkable dissimilarities are that the proposed objective function considers the robustness of estimation and a new stabilizing item is designed to achieve the numerical stability of a solution.

4. Solving the objective function

Eq. (23) is an unconstrained optimization problem. Compared to solving the traditional linearization model, the solving of Eq. (23) is challenging. As a result, finding an efficient numerical method with low computational complexity and cost is essential to successful applications of Eq. (23). In this section, the alternant iteration scheme and homotopy method are introduced, and an efficient algorithm that integrates the beneficial advantages of the both methods is described in detail.

Directly solving Eq. (23) is challenging because two unknown variables, G and B, need to be obtained. For ease of calculation, the alternant iteration scheme had been proposed in [30]. The key element behind the alternant iteration scheme is that variables G and B are obtained alternately, that is, in the kth step, if the value of variable G is given, then the estimation of variable B can be obtained by solving Eq. (23), and variable G can be recalculated using a suitable algorithm when B is fixed. Finally, repeating the above process, the estimation of the variables G and B can be achieved.

In this section, for conciseness of expression, the homotopy method is introduced according to variable G. The solving for variable B using the homotopy method is similar to that for variable G. According to the alternant iteration scheme, when the estimation of variable B is obtained in the kth step, minimizing Eq. (23) is equivalent to the solving of the following system of nonlinear equations [39]:

$$F(G) = 0 \tag{24}$$

where $F(G)$ is the gradient vector of Eq. (23) when variable B is known.

For the algorithms for solving a system of nonlinear equations, such as the Newton algorithm and the quasi-Newton methods, the iterative series $\{G^k\}$ may converge to the real solution G^* only when the initial values are sufficiently close to G^*. Unfortunately, providing a good initial value is still challenging in real ECT applications. As a result, finding an efficient algorithm where the numerical performances are not sensitive to the choice of the initial value will be highly desirable for real applications. In the past few years, a lot of effort has been devoted to developing such numerical methods and great advances have been made. One of the successes is the homotopy method, which has found wide application with excellent numerical performances. The homotopy method permits rather general initial values, not only those sufficiently close to the real solution G^*. In fact, the homotopy method can be applied to complicated systems where nothing is known about the solutions and where solutions are required to exist even if the coefficients in the equations are perturbed or the coefficients are inaccurate. More details on the homotopy method can be found in [40–42].

The general homotopy paradigm involves embedding the equations to be solved, $F(G) = 0$, in a system of equations of one higher dimension, $H(G, \lambda) = 0$, with the introduction of one more variable λ, called the homotopy parameter or continuation parameter. Typically, λ is restricted to the range [0, 1], and the embedding is done such that the augmented system $H(G, 0) = 0$ is easy to solve and reduces to the original system when $\lambda = 1$, i.e., $H(G, 1) = F(G)$. More details on the design of the homotopy equation can be found in [41,42]. In order to efficiently solve the homotopy equation, $\lambda \in [0, 1]$ can be divided into [40,42]

$$0 = \lambda_0 < \lambda_1 < \cdots < \lambda_N = 1. \tag{25}$$

At each point λ_i, solve the following discrete homotopy equation using a suitable algorithm:

$$H(G, \lambda_i) = 0, \quad i = 1, 2, \ldots, N. \tag{26}$$

Setting the solution $G(\lambda_i)$ as the initial value of the homotopy equation $H(G, \lambda_{i+1}) = 0$, repeat this process until $\lambda_i = 1$; the solution obtained is the final solution.

In this paper, the fixed point homotopy is employed for simplification of the computation, which can be expressed as follows:

$$(1 - \lambda_i)(G - G_0) + \lambda_i F(G) = 0. \tag{27}$$

For notational simplicity, Eq. (27) can be concisely reformulated as

$$G = \psi(G, \lambda_i) \tag{28}$$

where $\psi(\cdot)$ is a function of variables G and λ.

It is obvious that Eq. (28) is a system of nonlinear equations. In this work, the fixed point iterative algorithm is used to solve Eq. (28), which can be described as follows [41]:

$$G^{k+1} = \psi\left(G^k, \lambda_i\right). \tag{29}$$

It can be seen that the range of the solution is from 0 to 1. According to the prior information, consequently, the iterative scheme is slightly modified. As a result, a projected operator is introduced into this iterative scheme:

$$G^{k+1} = \text{Project}\left\{\psi\left(G^k, \lambda_i\right)\right\} \tag{30}$$

where

$$\text{Project}[g(x)] = \begin{cases} 0, & \text{if } g(x) < 0 \\ g(x), & \text{if } 0 \le g(x) \le 1 \\ 1 & \text{if } g(x) > 1. \end{cases} \tag{31}$$

5. Numerical simulations and discussion

According to the above discussion, the proposed image reconstruction method involves solving Eq. (23) using the homotopy method with the alternant iteration scheme, which can be referred to as the semiparametric reconstruction (SR) method. In this paper, numerical simulations are implemented to evaluate the numerical performances and effectiveness of the SR algorithm, and the quality of the reconstructed images is compared to those for the projected Landweber iteration (PLI) algorithm and the ART algorithm. All algorithms were performed using the MATLAB software.

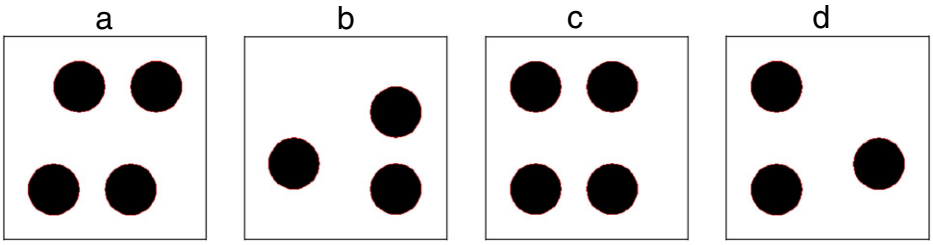

Fig. 2. Tested objects.

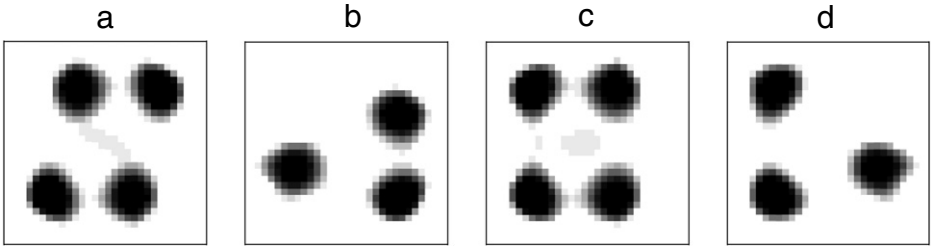

Fig. 3. Images reconstructed by the PLI algorithm.

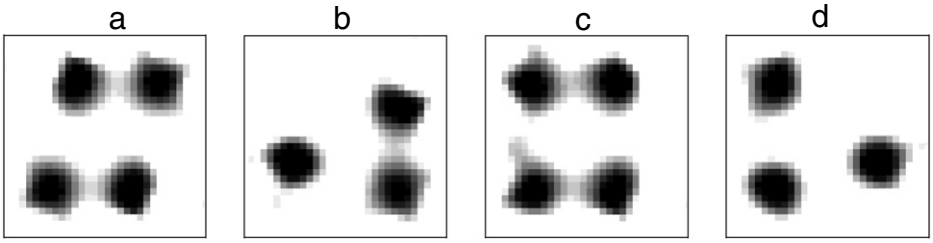

Fig. 4. Images reconstructed by the ART algorithm.

In the numerical simulations, a 12-electrode square sensor was employed and an image was presented using 32×32 pixels. Four permittivity distributions, which are shown in Fig. 2, were chosen for image reconstruction. The black color stands for the high permittivity materials with a value of 2.6, and the white color represents the low permittivity materials with a value of 1.0.

Initial images for the PLI algorithm, the ART algorithm and the SR algorithm were computed by the STR method, which can be defined as follows: $G = (S^T S + \alpha I)^{-1} S^T C$. The images reconstructed by the PLI algorithm and the ART algorithm are shown in Figs. 3 and 4, respectively. Tables 1 and 2 present the algorithmic parameters for the PLI algorithm and the ART algorithm, respectively. In the SR algorithm, we set $p_i = p$, $q_j = q\,(i = 1, 2, \ldots, n)$, $q = 1$, $\lambda = 1$, $\beta_1 = 1$, $\beta_2 = 1$, $\delta = 0.5$, and $u = 0.001$, and the values of p are selected according to a specific reconstruction task. The number of iterations is 6 for all cases. The rest of the algorithmic parameters for the SR algorithm are shown in Table 3. Fig. 5 shows the images reconstructed by the SR algorithm. The image error [17], which is presented in Table 4, is used to evaluate the quality of the reconstructed images.

Fig. 3 shows the images reconstructed by the PLI algorithm. It can be seen that the main advantages for the PLI algorithm involve the easy implementation and low computational complexity and cost. Unfortunately, the quality of the images reconstructed by the PLI algorithm is not satisfactory. The artifacts in the reconstructed images are not removed effectively and the distortions are relatively serious. These results also reveal that it is hard for the PLI algorithm to exactly reconstruct the original objects.

The images reconstructed by the ART algorithm are shown in Fig. 4. It can be seen that the advantages of the ART algorithm involve the easy implementation and the low computational complexity; however, the quality of the reconstructed images is far from perfect and the distortion of the reconstructed images is relatively large. These results indicate that it is hard for the ART method to ensure detailed information in the reconstructed images.

Fig. 5 shows the images reconstructed by the SR algorithm. As could have been expected, in all cases considered in this work, the SR algorithm shows excellent numerical performances. A dramatic improvement in the accuracy and spatial resolution in the reconstructed images is achieved, and the artifacts in the reconstructed images can be effectively eliminated. The reconstruction results also indicate that the SR algorithm is successful in solving ECT image reconstruction problems.

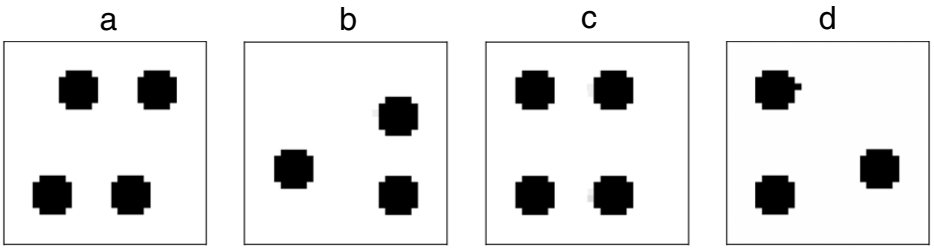

Fig. 5. Images reconstructed by the SR algorithm.

Table 1
Algorithmic parameters for the PLI algorithm.

Algorithmic parameters	Fig. 2(a)	Fig. 2(b)	Fig. 2(c)	Fig. 2(d)
Relaxation factor	1	1	1	1
Number of iterations	500	500	530	680

Table 2
Algorithmic parameters for the ART algorithm.

Algorithmic parameters	Fig. 2(a)	Fig. 2(b)	Fig. 2(c)	Fig. 2(d)
Relaxation factor	1	1	1	1
Number of iterations	400	400	405	360

Table 3
Algorithmic parameters for the SR algorithm.

Algorithmic parameters	Fig. 2(a)	Fig. 2(b)	Fig. 2(c)	Fig. 2(d)
p	0.5	0.5	0.5	0.4
α_1	0.2	0.2	0.2	0.2
α_2	0.01	0.01	0.01	0.01

Table 4
Image error (%).

Algorithms	Fig. 2(a)	Fig. 2(b)	Fig. 2(c)	Fig. 2(d)
PLI	18.98	17.64	18.84	17.57
ART	20.32	18.54	20.45	18.12
SR	0.15	0.26	0.80	3.64

Tables 1–3 present the algorithmic parameters for the PLI algorithm, the ART algorithm and the SR algorithm, respectively. It can be seen that the algorithmic parameters for the PLI algorithm and the ART algorithm are simpler than those for the SR algorithm, which indicates that the computational complexities of the PLI algorithm and the ART algorithm are lower than that of the SR algorithm. It is worth mentioning that the objective function in the SR algorithm can be simplified by selecting different parameters in real applications.

The image errors are shown in Table 4. The second and third rows give the image errors for the PLI algorithm and the ART algorithm, respectively. It can be observed that for the cases considered in this paper the accuracy of the images reconstructed by the PLI algorithm is slightly higher than that of the images reconstructed by the ART algorithm. The fourth row in Table 4 presents the image errors for the SR algorithm. It can be seen that for the reconstructed cases in this paper the SR algorithm gives the smallest image errors and a dramatic improvement in the accuracy is achieved, which indicates that the SR algorithm is successful in solving ECT image reconstruction problems.

6. Conclusions

Exactly reconstructing the original objects is highly desirable in ECT applications. In theory, ECT image reconstruction processes are discrete inverse problems with a finite number of parameters; methods that ensure the numerical stability of a solution while increasing the quality of the images reconstructed should be adopted. In this paper, a generalized image reconstruction model that simultaneously considers the inaccurate property in the measured capacitance data and the linearization approximation error is presented. A generalized objective function, which has been developed using a combinational M-estimation and an extended stabilizing item, is proposed. The objective function unifies six estimation methods into a concise formula, where different estimation methods can be easily obtained by selecting different

parameters. A homotopy method that integrates the beneficial advantages of the alternant iteration scheme is employed to solve the proposed objective function. Numerical simulations are implemented to evaluate the numerical performances and effectiveness of the proposed algorithm, and the numerical results reveal that the proposed algorithm is efficient and overcomes the problem of numerical instability in the process of ECT image reconstruction. For the reconstruction objects considered in this paper, a dramatic improvement in accuracy and spatial resolution can be achieved, which indicates that the proposed algorithm is a promising candidate for solving the ECT inverse problem.

Applications indicate that each algorithm has its pros and cons, and may show different numerical performances for different reconstruction objects owing to the ill-posed nature of the ECT image reconstruction problem. In real applications, the selection of an algorithm depends mainly on the prior information for a specific reconstruction problem and the measurement requirements. Our work provides an alternative approach for ECT image reconstruction, which should be further investigated in the future.

Acknowledgements

The authors wish to thank the National Natural Science Foundation of China (No. 50736002), the China Postdoctoral Science Foundation (No. 20090460263 and No. 201003088), the Fundamental Research Funds for the Central University (No. 10MG20), the Program for Changjiang Scholars and Innovative Research Teams in University (No. IRT0952) and the National High Technology Research and Development Program of China (No. 2007AA05Z331) for supporting this research.

References

[1] Yang W.Q., Liu S., Role of tomography in gas/solids flow measurement, Flow Measurement and Instrumentation 11 (2000) 237–244.
[2] A.J. Jaworski, T. Dyakowski, Application of electrical capacitance tomography for measurement of gas–solids flow characteristics in a pneumatic conveying system, Measurement Science and Technology 12 (2001) 1109–1119.
[3] M. Niedostatkiewicz, J. Tejchman, Z. Chaniecki, K. Grudzien, Determination of bulk solid concentration changes during granular flow in a model silo with ECT sensors, Chemical Engineering Science 64 (2009) 20–30.
[4] J.C. Gamio, J. Castro, L. Rivera, J. Alamilla, F. Garcia-Nocetti, L. Aguilar, Visualisation of gas–oil two-phase flows in pressurized pipes using electrical capacitance tomography, Flow Measurement and Instrumentation 16 (2005) 129–134.
[5] J. Wiens, T. Pugsley, Tomographic imaging of a conical fluidized bed of dry pharmaceutical granule, Powder Technology 169 (2006) 49–59.
[6] S. Liu, Q. Chen, H.G. Wang, F. Jiang, I. Ismail, W.Q. Yang, Electrical capacitance tomography for gas–solids flow measurement for circulating fluidized beds, Flow Measurement and Instrumentation 16 (2005) 135–144.
[7] Y. Makkawi, R. Ocone, Integration of ECT measurement with hydrodynamic modeling of conventional gas–solid bubbling bed, Chemical Engineering Science 62 (2007) 4304–4315.
[8] S. Liu, W.Q. Yang, H.G. Wang, F. Jiang, Y. Su, Investigation of square fluidized beds using capacitance tomography: preliminary results, Measurement Science and Technology 12 (2001) 1120–1125.
[9] M.A. Bennett, R.M. West, S.P. Luke, R.A. Williams, The investigation of bubble column and foam processes using electrical capacitance tomography, Minerals Engineering 15 (2002) 225–234.
[10] K. Zhu, R. Madhusudana, C.H. Wang, S. Sundaresan, Electrical capacitance tomography measurements on vertical and inclined pneumatic conveying of granular solids, Chemical Engineering Science 58 (2003) 4225–4245.
[11] C.G. Xie, S.M. Huang, B.S. Hoyle, R. Thorn, C. Lenn, D. Snowden, M.S. Beck, Electrical capacitance for flow imaging: system model for development of image reconstruction algorithms and design of primary sensors, IEE Proceedings G 139 (1992) 89–98.
[12] A.N. Tikhonov, V.Y. Arsenin, Solution of Ill-posed Problems, V.H. Winston & Sons, 1977.
[13] J.J. Liu, The Regularization Methods of Ill-posed Problems and Applications, Science Press, Beijing, 2005.
[14] W.Q. Yang, D.M. Spink, T.A. York, H. McCann, An image reconstruction algorithm based on Landweber's iteration method for electrical capacitance tomography, Measurement Science and Technology 10 (1999) 1065–1069.
[15] S. Liu, L. Fu, W.Q. Yang, Optimization of an iterative image reconstruction algorithm for electrical capacitance tomography, Measurement Science and Technology 10 (1999) L37–L39.
[16] J.D. Jang, S.H. Lee, K.Y. Kim, B.Y. Choi, Modified iterative Landweber method in electrical capacitance tomography, Measurement Science and Technology 17 (2006) 1909–1917.
[17] W.Q. Yang, L.H. Peng, Image reconstruction algorithms for electrical capacitance tomography, Measurement Science and Technology 14 (2003) L1–L13.
[18] B.L. Su, Y.H. Zhang, L.H. Peng, D.Y. Yao, B.F. Zhang, The use of simultaneous iterative reconstruction technique for electrical capacitance tomography, Chemical Engineering Journal 77 (2000) 37–41.
[19] C.H. Mou, L.H. Peng, D.Y. Yao, D.Y. Xiao, Image reconstruction using a genetic algorithm for electrical capacitance tomography, Tsinghua Science and Technology 10 (2005) 587–592.
[20] M. Takei, GVSPM image reconstruction for capacitance CT images of particles in a vertical pipe and comparison with the conventional method, Measurement Science and Technology 17 (2006) 2104–2112.
[21] M. Soleimani, W.R.B. Lionheart, Nonlinear image reconstruction for electrical capacitance tomography using experimental data, Measurement Science and Technology 16 (2005) 1987–1996.
[22] H.X. Wang, L. Tang, Z. Cao, An image reconstruction algorithm based on total variation with adaptive mesh refinement for ECT, Flow Measurement and Instrumentation 18 (2007) 262–267.
[23] W.F. Fang, A nonlinear image reconstruction algorithm for electrical capacitance tomography, Measurement Science and Technology 15 (2004) 2124–2132.
[24] C. Ortiz-Aleman, R. Martin, J.C. Gamio, Reconstruction of permittivity images from capacitance tomography data by using very fast simulated annealing, Measurement Science and Technology 15 (2004) 1382–1390.
[25] Q. Marashdeh, W. Warsito, L.S Fan, F.L. Teixeira, Non-linear image reconstruction technique for ECT using a combined neural network approach, Measurement Science and Technology 17 (2006) 2097–2103.
[26] W. Warsito, L.S. Fan, Neural network based multi-criterion optimization image reconstruction technique for imaging two- and three-phase flow systems using electrical capacitance tomography, Measurement Science and Technology 12 (2001) 2198–2210.
[27] S. Liu, L. Fu, W.Q. Yang, H. Wang, F. Jiang, Prior on-line iteration for image reconstruction with electrical capacitance tomography, IEE Proceedings—Science, Measurement and Technology 151 (2004) 195–200.
[28] M. Soleimani, P. Yalavarthy, H. Dehghani, Helmholtz-type regularization method for permittivity reconstruction using experimental phantom data of ECT, IEEE Transactions on Instrumentation and Measurement 59 (2010) 78–83.

[29] M. Soleimani, C.N. Mitchell, R. Banasiak, R. Wajman, A. Adler, Four-dimensional electrical capacitance tomography imaging using experimental data, Progress in Electromagnetics Research—PIER 90 (2009) 171–186.
[30] G.X. Chai, S.Y. Hong, The Semiparametric Regression Model, Anhui Publishing Group, Hefei, 1995.
[31] Y.H. Liu, L.J. Song, Ridge estimation method for ill conditioned semiparametric regression model, Hydrographic Surveying and Charting 28 (2008) 1–3.
[32] T.Y. Xiao, S.G. Yu, Y.F. Wang, Numerical Methods of the Inverse Problems, Science Press, Beijing, 2003.
[33] Y.F. Wang, Computational Methods for Inverse Problems and Their Applications, Higher Education Press, Beijing, 2007.
[34] P.J. Huber, Robust Statistics, John Wiley&Sons, New York, 1981.
[35] T. Wang, Methods on robust estimation and detection of multiple outliers in linear regression, Ph.D. Dissertation, The Fourth Military Medical University, 2000.
[36] Y. Dodge, J. Jureckova, Adaptive Regression, Springer-Verlag, New York, 2000.
[37] T. Hebert, R. Leahy, A generalized EM algorithm for 3-D Bayesian reconstruction from Poisson data using Gibbs priors, IEEE Transactions on Medical Imaging 8 (1989) 194–202.
[38] R. Acar, C.R. Vogel, Analysis of bounded variation penalty methods for ill posed problem, Inverse Problems 10 (1994) 1217–1229.
[39] M.T. Heath, Scientific Computing: An Introductory Survey, Tsinghua University Press, Beijing, 2001.
[40] Z.H. Ma, Handbook of Modern Applied Mathematics, Tsinghua University Press, Beijing, 2005.
[41] X.D. Huang, Z.G. Zeng, Y.N. Ma, Theory and Methods for Nonlinear Numerical Analysis, Wuhan University Press, Wuhan, 2004.
[42] Q.Y. Li, Z.H. Mo, L.Q. Qi, Numerical Methods of System of Nonlinear Equations, Science Press, Beijing, 1987.